Romanian Reports in Physics, Vol. 68, No. 4, P. 1513–1522, 2016

AN AFM AND SEM STUDY OF A DENTAL RESTORATION MATERIAL GRAIN STRUCTURE

D. CHICEA[1,2]

[1] University "Lucian Blaga" of Sibiu, Physics Dept., Dr. Ion Ratiu Str. 7–9, Sibiu, 550012, Romania, E-mail: dan.chicea@ulbsibiu.ro
[2] Pediatric Respiratory Medicine Research Center (CCMRP), University Lucian Blaga of Sibiu

Received August 17, 2015

Abstract. An AFM and SEM study of the Charisma Opal, a frequently used dental restoration material, was conducted to investigate the grain structure and distribution, which strongly dictate its mechanical properties. The AFM technique was used to investigate the distribution of the smaller particles, with diameters below 70 nm, while the SEM was use to investigate the bigger particles, with diameters ranging up to 1600 nm. A simple data processing procedure for 3D surface imaging of SEM topography data is presented, as well. The results reveal that Charsima Opal is a hybrid combination of both micro and nanostructured material.

Key words: charisma opal, AFM, SEM, grain analysis.

1. INTRODUCTION

Dental composite resins (CR) represent a class of materials that are currently used in dental restauration. The composite material consists of the resin matrix, which gives plasticity and filler particles that confer hardness and strength. The combination presents certain properties needed for withstanding the particular mechanical and biochemical conditions currently found in the oral cavity. The plastic phase hardening occurs at visible light exposure and is the consequence of the cross-linking of the resin monomers that form the polymer network [1].

The hardness of the composite depends of both the organic matrix and its structure [2]. The resin composite degree of conversion depends of the type of monomer and of the amount of photoinitiators, and it is one of the factors that affect the hardness of the material. References [3–5] state that a higher degree of conversion is associated with a higher composite hardness. Reference [6] though presents the results of a study on three resin composites. One of them was Tetric EvoCeram (Ivoclar Vivadent, Liechtenstein), a nano-hybrid material; the second was IPS Empress Direct (Ivoclar Vivadent), a nanohybrid material, as well, and the third one was Charisma Opal (Heraeus Kulzer, Germany), a submicron hybrid material [6]. The study reveals that Charisma Opal, in spite of having the highest degree of conversion exhibited the lowest hardness [6]. The above mentioned rule

[3–5] was changed by the insertion of nanocomposites and this suggests that hardness at micron and submicron scale is influenced by the filler amount and composition more than it is by the degree of conversion [7].

The role of grain size in surface cracking, not only in composite resins but in other materials as well, has been investigated by many authors. Reference [8] for instance investigated steel specimens with four different grain sizes under heavy forging, using scanning electron microscopy. They report that "cracks were formed at grain boundaries mainly and at junctions between three grains that have big Taylor factors values" [8]. Consequently the authors conclude that material with bigger grain size cracks more easily as it has a smaller number of grain boundaries [8]. Similar results were reported on different materials, though, as yttria-stabilized zirconia polycrystalline (Y-TZP) ceramics, materials that are frequently used in dental restauration [9]. The authors used microwave sintering that had the direct effect of producing a finer grain structure that improved the mechanical properties of the ceramics [9].

Other authors [10] investigated resin composites containing Ba-Si-Al glass particles as filler, both micron and submicron sized. The filler particles were investigated using X-ray granulometry and the polymerized composite resins in terms of mechanical properties, like strengths, hardness, flexural strength, and creep. The authors reported that the composites were similar regarding flexural strength and creep but the resins with submicron filler particles had lower flexural modulus and were harder [10]. Another class of materials currently used in dentistry consists of zirconia-silica glass ceramics. Reference [11] reports on using a sol-gel method to synthesize nanostructured zirconia-silica glass ceramics for dental use. The authors report that the material had a bigger hardness and a lower elastic modulus than the lithium disilicate [11]. The material also presented a bigger fracture toughness.

Feldspathic dental porcelain represents another class of materials currently used in dental restoration. Reference [12] reports that this type of material presents a relatively high flexural strength and the authors attribute this feature to the fine grain size of the material.

The above mentioned references reveal that grain size and distribution appears to have a crucial role in selecting a proper material for dental restoration, as certain mechanical properties as hardness and flexural strength are required to be in a specific range.

An already traditional technique for investigating the grain size of a material is X rays diffraction [13]. The Scherrer equation [14] states a relation between the full width of a peak corresponding to specific phase, at half of the maximum, and the mean crystallite size. The X rays powder diffraction works for crystalline materials only, while composite resins present amorphous phase, therefore this technique appears to be unfit for grain structure analysis on composite resins.

Scanning electron microscopy (SEM) is currently used in characterizing the grain structure of different type of materials. Literature is abundant in reports on

this subject and [8, 12] are just some of them, which have already been cited in this work.

Another technique, newer though, which has been successfully used in visualizing surface details and in performing grain size analysis is the atomic force microscopy, AFM. References [15–17], to mention just a few, report on nanoparticle sizing using the AFM technique.

Charisma Opal (Heraeus Kulzer, Germany), is a resin composite containing Barium Aluminium glass and highly dispersive silica particles as filler. As the grain structure and distribution of the composite resin appears to be important in dictating the mechanical properties of a material, this work was carried on to investigate the grain structure of this composite resin by AFM and SEM, as part of an ongoing study.

2. MATERIAL AND METHODS

2.1. SAMPLE PREPARATION

The sample was deposited on glass microscope slides, 22 × 22 × 0.2 mm, as a drop, 1 mm thick, for AFM study. The samples were exposed for 20 s to the light beam a lamp (Heraeus Kulzer Translux) in order to have the base resin polymerized.

The same procedure was followed to prepare the samples for SEM imaging, except that the typical Aluminum sample holder for Phenom SEM microscopes was used as substrate instead of the thin microscope slide.

2.2. AFM IMAGING AND GRAIN STRUCTURE ANALYSIS

The AFM belongs to the class of scanning probe microscopes. A detailed presentation on the procedure for acquiring the topography data and for reconstructing the image is presented in [17] and [18], among many others. An Agilent 5500 AFM was used in the work presented here. The scanning mode was AAC. Cantilevers of type N9621 having the constant between 21 and 98 N/m were used and the resonance frequency, selected by auto-tuning, was 161.868 KHz. More details on the scanning procedure are presented in [17] and [19].

Several scans with lower resolutions were carried on and several areas were selected. Bigger resolution scans, (512 × 512 pixels) of a 1.2 × 1.2 μm^2 were carried and the topography information was acquired.

The topography acquired data was processed using Gwyddion 2.41. First the scar removal tool was used followed by fixing the minimum value to zero.

After these basic operations were performed, a grain statistics was carried on, using the grain distribution feature, implemented in Gwyddion 2.41, based on [20] and [21]. First the grains have to be marked and this was done using the so called

"watershed" algorithm. Details on this type of data processing are presented in [19], where the grains were marked using the Laplaceian algorithm instead. After marking the grains a statistics was done using the same Gwyddion 2.41.

Another type of data processing was done using the grain distribution feature of the above mentioned software. The equivalent disk radius of each grain was calculated. This feature uses the projection of the grain area on the horizontal plane and assumes the area to be circular.

2.3. SEM IMAGING AND GRAIN STRUCTURE ANALYSIS

The SEM belongs to the class of scanning probe microscopes, as the AFM does, as well. The samples were scanned using a Phenom ProX SEM, with an accelerating voltage of 10 kV, producing a magnification of 10000×.

The image processing was carried on using ImageJ 1.48V [22]. The data processing procedure requires several steps. First the grains are marked by threshold [22, 23, 24]. The Intermodes method was chosen with color set to white and a triggering value of 127 in a range from 0–255. Next, measurements to be performed need to be set. As we are interested in grain or particle statistics, area was selected as parameter. Special care was taken to analyze only the particles marked by threshold. This type of data processing is similar with the algoritm used in AFM data processing.

3. RESULTS

3.1. AFM ANALYSIS RESULTS

The 3D topography image of one of the selected areas is presented in Fig. 1.

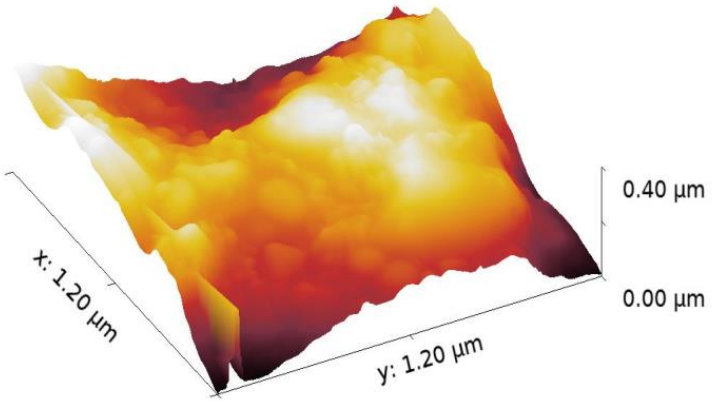

Fig. 1 – The 3D topography of the composite resin deposited on a microscope glass slide.

Figure 2 presents the distribution of the equivalent grain disk radius for the collection of topography values presented in Fig. 1. The equivalent disk radius is the radius of a disk having the same area as the projection of the grain to the horizontal surface.

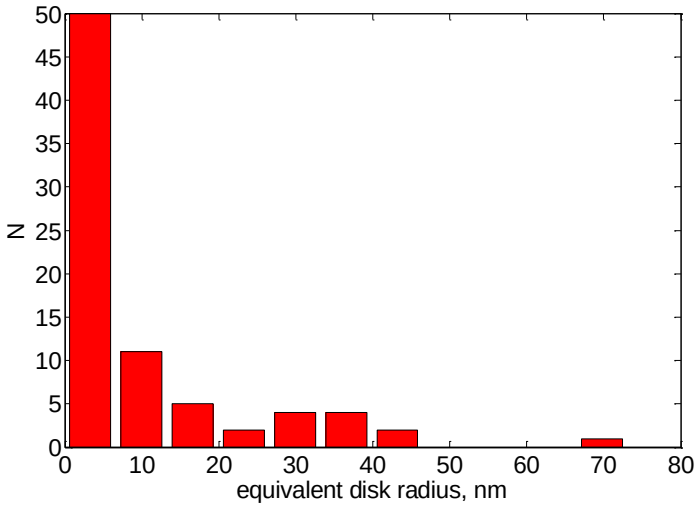

Fig. 2 – The distribution of the equivalent grain disk radius.

As pointed out in [16, 17] and [19] the AFM involves scanning details with a tip that has a diameter that is increasing during scanning and can soon reach 40 nm. For this reason the results produced in tapping mode, as used in the work presented here, for nonoconductive samples, cannot be considered accurate when rendering details considerably smaller than the tip diameter. With this in mind, the first two bins of the distribution presented in Fig. 2 were disregarded and a weight average over the data contained in the other 9 bins was computed. We found that the average disk radius was 30.6 nm, therefore the average disk diameter, considered to be the average grain size, was found to be 61.2 nm.

3.2. SEM ANALYSIS RESULTS

An image acquired using the above mentioned parameters is presented in Fig. 3. The image in Fig. 3 covers an area on the sample of 26.8 × 26.8 μm^2, with a resolution of 1024 × 1024 pixels. This makes the side of one square pixel on the image to be 26.1719 nm and one micron to be stretching over 38.209 pixels on image.

The image of Fig. 3 with the particles marked by threshold, having the contour highlighted, is presented in Fig. 4.

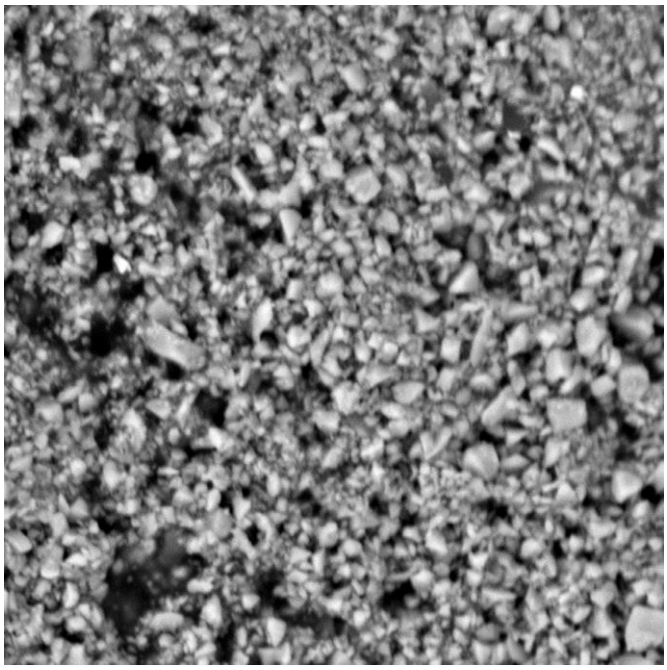

Fig. 3 – A topography SEM image acquired using an electron beam accelerated at 10 kV.

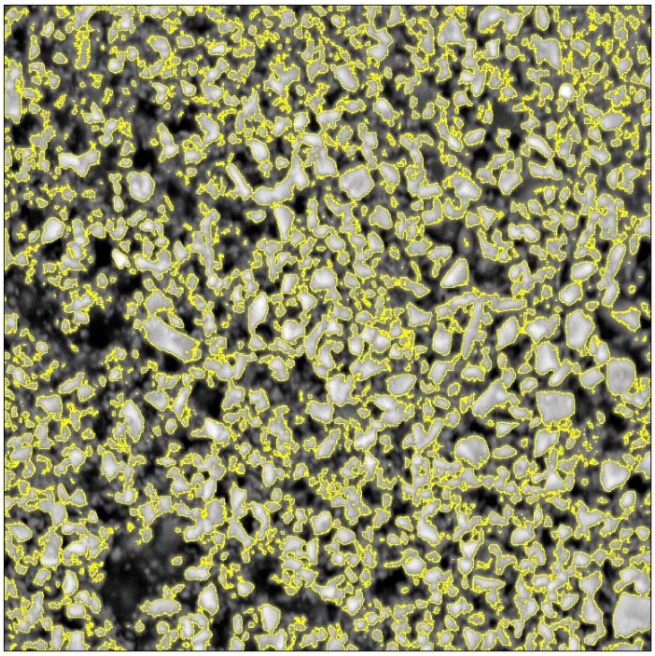

Fig. 4 – The image in Fig. 3 with the particles marked by threshold, having the contour highlighted.

Particle analysis was carried on and the parameters of each individual identified particle are extracted; area in our case. We found that the average particle area was 0.154 μm^2. In order to estimate the size of the particles from the SEM image we can consider the particles to have a circular projection on the plane perpendicular to the electron beam, as the image is. We found the average diameter of the particles, assumed to be the particle size, to be 0.305 μm. After computing the equivalent diameter of each particle the standard deviation of the values was computed and found to be 0.322 μm. A plot revealing the size distribution of the particles from the SEM image is presented in Fig. 5. We notice that the first bin of the histogram contains considerably more particles than the rest of the histograms. This is consistent with the resolution of the SEM image, that is 26.17 nm per pixel, which makes all the small grains stretching over a very few pixels to fall in the first bin. This small grains are the grains in the size range that was rendered by the AFM technique.

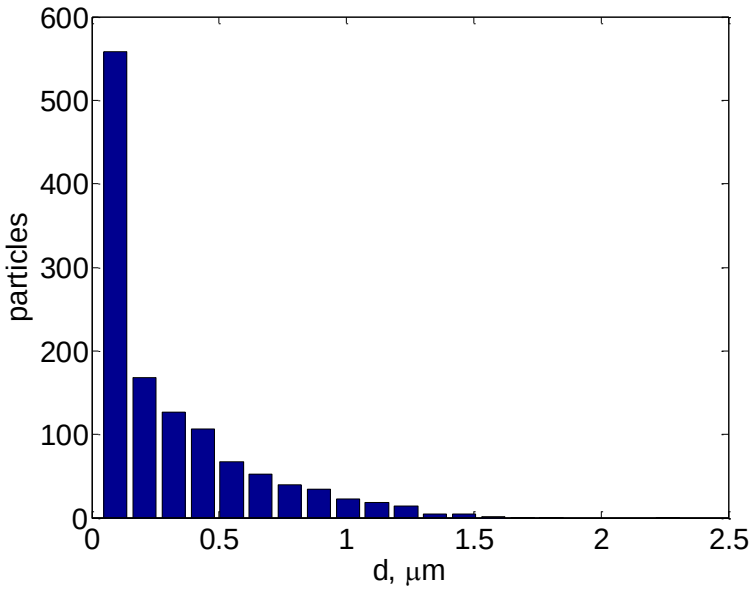

Fig. 5 – The distribution of the particles by their diameter.

The SEM topography can be processed to produce a 3D image, after converting it to a grayscale type. The lighter is the area on the sample, the bigger is the value of the intensity. This makes possible a conversion of the plane image, each pixel having a certain value of the intensity, to a 3D plot where the height of each pixel is proportional to the intensity value corresponding to it. Such a processed image is presented in Fig. 6, where an area of 100 × 100 pixels, hence of 2.793 μm × 2.793 μm is rendered in a 3D plot.

4. DISCUSSIONS AND CONCLUSION

Grain size and distribution dictate several mechanical properties as hardness and flexural strength. These mechanical properties are required to be in a specific range for a composite resin to be a proper material for dental restoration, among other properties [25]. Two essentially different physical procedures for investigating the grain size of a composite resin used for dental restauration, Charisma Opal, were used in the work described here: AFM and STM.

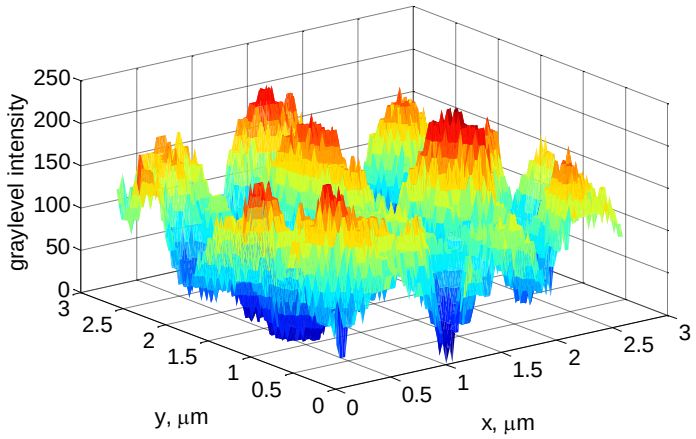

Fig. 6 – 3D plot of an area of 100 × 100 pixels, hence of 2.793 μm × 2.793 μm.

AFM in tapping mode, with a relatively stiff cantilever, proper for harder materials, was used to scan a smaller area, 1.2×1.2 μm^2, with a resolution of 512×512 pixels. The topography information was processed using Gwyddion 2.41. The equivalent disk statistics was carried on, and the equivalent disk radius distribution revealed that most of the grains had the disk radius smaller than 10 nm. The distribution presents a wide maximum centered on 33 nm. The very high part of the small values of the distribution can be interpreted as a possible artifact and its height and shape should be viewed with caution. The artifact can possible be caused by the systematic scanning error of the AFM procedure, where the tip, soon after the beginning of the scanning process, has a diameter bigger around 40 nm, much bigger than the possible nanosized grains, which appear to be smaller than 10 nm. Additional explanation in support of this statement can be found in detail in [16] and [19]. The equivalent disk radius distribution peak centered on 33 nm, with the average disk diameter, after disregarding the small particles groups, as presented in 3.1, of 61.2 nm, are consistent with the composite resin description by the producer [25], which states that the composite is based on a BIS-GMA matrix and contains 58 % filler consisting of Barium Aluminium glass, 0.02–2 μm, and highly dispersive silica, 0.02–0.07 μm. What we found using AFM was the

distribution of the silica particles and the small size part of the distribution of the Barium Aluminium glass.

The SEM was used to scan a bigger area, 26.8 × 26.8 μm. As the area was bigger, the details that could be investigated were bigger, as well. A different software, for image processing, ImageJ, was used to produce the distribution of the equivalent radius of the particles on the image, based on processing the intensity of the almost-back scattered electrons converted into gray levels. The distribution reveals that most of the particles have an equivalent diameter smaller than 0.1 μm. This result is consistent with the composite resin description by the producer [26] and includes the highly dispersive silica particles. A big decrease can be noticed to the next group, with particles in the range 0.1–0.2 μm followed by a smaller decrease as we move to the range up to 1.8 μm, group consisting of Barium aluminium glass, 0.02–2 μm, as stated by producer.

The results of the work presented here are similar with the results reported on AFM and SEM investigation of other composite resins. Reference [27] investigated fiber-reinforced polymer composite resin, used as archwire, both using AFM and Field Emission SEM. The AFM images presented in [27] reveal details on the surface with the size of the grain projection to the horizontal plane starting below 1 μm and up to several microns. The maximum height on the AFM images was 5 μm on one image and 2 μm on the other one, which confirms that the grains diameter were less than a few microns. The resins were Translucent Archwire, not Charisma Opal, therefore differences in the filler materials are normal.

Another reference reporting on AFM and SEM analysis of composite resins is [28]. It was phenolic resin with Sisal fiber as reinforcing material. The SEM was used on bigger area, in order to investigate the bigger details on the surface, as in the work reported here. The SEM images in [27] reveal that the fibers were around 7 μm in diameter. The AFM was used to investigate the smaller details on the surface [28], as in the work reported here, and the SEM images reveal details of the order of 20–50 nm.

The results presented in this work reveal that two methods, AFM and SEM, using different physical procedures, can be used in a complimentary manner to investigate composite materials, containing grains with sizes in the range from nanometers to microns.

Acknowledgements. I am grateful to Professors Laura Ștef, MD, PhD and Boța Gabriela, MD, PhD, of the University Lucian Blaga of Sibiu, for providing the samples and for fruitful discussions. I am also especially indebted to Total Spectrum SRL, Romania, for providing access to the Phenom ProX SEM.

The work presented here was partially supported by the ULBS internal research grant LBUS-IRG-2015-01.

REFERENCES

1. Z. Tarle, A. Knezevic, D. Matosevic, D. Skrtic, M. Ristic, K. Prskalo, S. Music, J. Mol. Struct. **924–926**, 161–165 (2009).
2. M.N. Mandikos, G.P. McGivney, E. Davis, P.J. Bush, J.M. Carter, J. Prosthet. Dent. **85**, *4*, 386–395 (2001).
3. S.G. Pereira, R. Osório, M. Toledano, T.G. Nunes, Dent. Mater. 21, *9*, 823–830 (2005).
4. Y.H. Kwon, G.H. Jeon, C.M. Jang, H.J. Seol H.I. Dim, J. Biomed. Mater. Res. Part B, Appl Biomater. **76**, *1*, 106-113 (2006).
5. J. Manhart, K.H. Kunzelmann, H.Y. Chen, R. Hickel, J Biomed Mater Res. **53**, *4*, 353–361 (2000).
6. D. Marovic, V. Panduric, Z. Tarle, M. Ristic, K. Sariri, N. Demoli, E. Klaric, B. Jankovic, K. Prskalo, Journal of Molecular Structure **1044**, 299–302 (2013).
7. A.D. Neves, J.A. Discacciati, R.L. Orefice, W.C. Jansen, Pesqui. Odontol. Bras. **16**, 349–354 (2002).
8. Z.H. Wang, S.H. Sun, B. Wang, Z.P. Shi, W.T. Fu, Materials Science and Engineering A **625**, 321–330 (2015), doi: 10.1016/j.msea.2014.12.022.
9. A. Presenda, M.D. Salvador, F.L. Penaranda-Foix, R. Moreno, A. Borrell, Ceramics International **41**, *5*, 7125–7132 (2015), doi: 10.1016/j.ceramint.2015.02.025.
10. L.L. Valente, S.L. Peralta, F.A. Ogliari, L.M. Cavalcante, R.R. Moraes, Dental Materials **29**, *11*, 1182–1187 (2013), doi: 10.1016/j.dental.7013.09.006.
11. C. Persson, E. Unosson, I. Ajaxon, J. Engstrand, H. Engqvist, W. Xia, Journal of the European Ceramic Society **32**, *16*, 4105–4110 (2012); DOI: 10.1016/j.jeurceramsoc.2012.06.028.
12. G.D. Quinn, K. Hoffman, J.B. Quinn, Dental Materials **28**, *5*, 502–511 (2012); DOI: 10.1016/j.dental.2011.12.005.
13. A. W. Hull, A new method of chemical analysis, J. Am. Chem. Soc. **41**, *8*, 1168–1175 (1919), DOI:10.1021/ja02229a003.
14. A.L. Patterson, Phys. Rev. **56**, *10*, 978–982 (1939); DOI:10.1103/PhysRev.56.978.
15. F. Zhang, S.W. Chan, J. E. Spanier, E. Apak, Q. Jin, R. D. Robinson, I. P. Herman, Appl. Phys. Lett. **80**, *27* (2002); DOI:10.1063/1.1430502.
16. D. Chicea, Optoelectronics and Advanced Materials – Rapid Communications **4**, *9*, 1310–1315 (2010).
17. D.Chicea, Romanian Reports in Physics **66**, *3*, 778–787 (2014).
18. http://www.jpk.com/general-scanning-probe-microscopy.431.html (as retrieved on June 23rd, 2015).
19. D. Chicea, B. Neamtu, R. Chicea, L.M. Chicea, Digest Journal of Nanomaterials and Biostructures **5**, *4*, 1015–1022 (2010).
20. P. Klapetek, I. Ohlídal, D. Franta, A. Montaigne-Ramil, A. Bonanni, D. Stifter, H. Sitter, Acta Physica Slovaca **3**, 223–230 (2003).
21. L. Vincent, P. Soille, IEEE Transactions on Pattern Analysis and Machine Intelligence **13**, 583–598 (1991).
22. W.S. Rasband, ImageJ, U.S. National Institutes of Health, Bethesda, Maryland, USA, imagej.nih.gov/ij/, 1997–2012.
23. M.D. Abràmoff, P.J. Magalhães, S.J. Ram, Biophotonics International **11**, *7*, 36–42 (2004).
24. C.A. Schneider, W.S. Rasband, K.W. Eliceiri, Nature Methods **9**, *7*, 671–675 (2012).
25. R.L. Bowen, The Journal of the American Dental Association, **66**, *1*, 57–64 (1963), doi:10.14219/jada.archive.1963.0010.
26. http://webmedia.kulzer-dental.com/media/hkg/downloads_new/charisma_4/charisma_diamond/Charisma_Family_PI_GB_Master.pdf (as retreived on June 30, 2015).
27. Chng C.K., Foong K., Gandedkar N.H., Chan Y.H., Chew C-L., Progress in Orthodontics **15**, *39*, 2014; DOI:10.1186/s40510-014-0039-8; http://www.progressinorthodontics.com/content/15/1/39.
28. Zhong L, Fu S., Li F., Zhan H., BioResources **5**, *4*, 2431–2446 (2010).